

Electronic structure, mechanical and thermodynamic properties of ThN from first-principles calculations

Yong Lu,^{1,2} Da-Fang Li,¹ Bao-Tian Wang,^{1,3} Rong-Wu Li,² and Ping Zhang^{1,4,*}

¹*LCP, Institute of Applied Physics and Computational Mathematics,
Beijing 100088, People's Republic of China*

²*Department of Physics, Beijing Normal University,
100875, People's Republic of China*

³*Institute of Theoretical Physics and Department of Physics,
Shanxi University, Taiyuan 030006, People's Republic of China*

⁴*Center for Applied Physics and Technology,
Peking University, Beijing 100871, People's Republic of China*

Abstract

Lattice parameter, electronic structure, mechanical and thermodynamic properties of ThN are systematically studied using the projector-augmented-wave method and the generalized gradient approximation based on the density functional theory. The calculated electronic structure indicates the important contributions of Th 6*d* and 5*f* states to the Fermi-level electron occupation. Through Bader analysis it is found that the effective valencies in ThN can be represented as Th^{+1.82} N^{-1.82}. Elastic constant calculations shows that ThN is mechanically stable and elastically anisotropic. Furthermore, the melting curve of ThN is presented up to 120 GPa. Based on the phonon dispersion data, our calculated specific heat capacities including both lattice and conduction-electron contributions agree well with experimental results in a wide range of temperature.

PACS numbers: 71.27.+a, 71.15.Mb, 71.20.-b, 63.20.dk

*Author to whom correspondence should be addressed. E-mail: zhang_ping@iapcm.ac.cn

I. INTRODUCTION

Actinide nitrides have been extensively studied in experiments in connection with their potential applications in the Generation-IV reactors [1]. These reactors raise a number of concerns surrounding the issue of nuclear power. The effective utilization of nuclear power will require continued improvements in nuclear technology, particularly related to safety and efficiency. Nowadays, except for the oxide based fuels, the nitride fuels also participate in the competition to become the alternative materials for their superior thermophysical properties, such as high melting point, high thermal conductivity, and high density, as well as the good compatibility with the coolant (liquid sodium) [2–5]. Since the high density of nitride fuels can bring out more excess neutrons, therefore, they have a higher potential to transmute the long lived fission products. As for reprocessing feasibility, actinide nitrides also appear to be a compromise between oxide and metal fuels. For the sake of better understanding of the behavior of these materials under irradiation, their accurate electronic structure description by first-principles methods is necessary. Actinides form an isostructural series of mononitrides with a simple rock-salt type structure and a complete solid solubility in the whole composition range. In virtue of the prospective use of actinide mononitrides as advanced fuel materials, it is of crucial importance to know their thermal properties for modeling the fuel behavior at elevated temperatures. The thermodynamic properties such as standard enthalpies of formation and heat capacities are essential to predict the phase stability including the melting points.

Despite the abundant research on actinide mononitride, however, for ThN compound, relatively little is known regarding its chemical bonding, mechanical properties, high pressure melting points, and phonon dispersion. In the early theoretical studies, only the lattice parameters and bulk modulus of the actinide nitride series have been calculated by utilizing linear muffin-tin orbital (LMTO) method [6]. Although the electronic properties and chemical bonding in ThN have been recently calculated by Shein *et al.* [7] through the full-potential linear-augmented-plane-wave (FLAPW) method, the study of the bonding nature of Th-N ionic/covalent character is still lacking. These facts, as a consequence, inhibit the fundamental understanding of thorium mononitride from basic point of view. Motivated by these observations, in this paper, we present a first-principles density functional theory (DFT) study by calculating the structural, electronic, mechanical, and thermodynamic

properties of ThN. As will be shown, a preliminary study of some bulk properties of ThN indicates that the conventional generalized gradient approximation (GGA) for the exchange-correlation potential in DFT can give satisfactory results when compared to experimental data and thus does not require other treatments beyond LDA/GGA such as LDA/GGA+ U , which are indispensable in the uranium and plutonium compounds for stronger localization and correlation of their $5f$ electrons.

After optimizing the ground state structure of ThN, we performed the calculation of density of states (DOS) and Bader analysis [8] for ThN. The results indicate that the Th $5f$ states are involved in the formation of Th-N and Th-Th interatomic bonds and about 1.82 electrons transfer from each Th atom to its surrounding N atoms. Through the mechanical analysis, we find that NaCl-style ThN is mechanically stable and elastically anisotropic. In order to predict the melting curve, we calculated the elastic constants, bulk modulus and shear modulus from ambient pressure to 117 GPa. Since we have known that ThN melts congruently at $2790\pm 30^\circ$ under a nitrogen pressure somewhat less than 1 atm [9], thus the ThN can be ranked as refractory materials. Utilizing the Lindemann melting criterion [10], we got the melting curve versus pressures. The melting points were enhanced by about 2100 K from ambient pressure to 117 GPa. Our predicted results indicate that ThN is able to withstand temperatures above 5100 K without chemical change and physical destruction under high pressures. The calculated phonon dispersion confirms the dynamic stability for ThN. Based on our phonon dispersion data, the lattice vibration energy, thermal expansion, and specific heat are obtained by using the quasiharmonic approximation (QHA). Our calculated special heat, including both lattice and conduction electron contributions, agrees well with experimental results at $T < 1500$ K domain.

The rest of this paper is organized as follows. The first-principles computational details are briefly introduced in Sec. II. The calculated results are presented and discussed in Sec. III. Finally, a summary of this work is given in Sec. IV.

II. COMPUTATIONAL METHODS

The first-principles total energy calculations were carried out using the Vienna *ab initio* simulations package (VASP) [11] with the projected-augmented-wave (PAW) pseudopotentials [12] and plane waves. The exchange and correlation effects were described within GGA

TABLE I: Strains used to calculate the elastic constants of NaCl-type ThN.

Strains	Parameters (unlisted: $\varepsilon_{ij}=0$)	$\frac{1}{V} \frac{\partial^2 E(V,\delta)}{\partial \delta^2} \Big _{\delta=0}$
1	$\varepsilon_{11}=\delta$	$C_{11} - P$
2	$\varepsilon_{11}=\varepsilon_{22}=\delta$	$2(C_{11}+C_{12} - P)$
3	$\varepsilon_{13}=\varepsilon_{31}=\delta$	$4C_{44} - 2P$

[13]. The thorium $6s^27s^26p^66d^15f^1$ and nitrogen $2s^22p^3$ electrons were treated as valence electrons. The electron wave function was expanded in plane waves up to a cutoff energy of 500 eV. We have performed numerous convergence tests on determining the influence of the k -point mesh on the total energy. The Monkhorst-Pack [14] $11 \times 11 \times 11$ mesh was used in Brillouin zone (BZ) integration, which turns to be sufficient to get results converged to less than 1.0×10^{-4} eV per atom. The corresponding electronic density of states (DOS) was obtained with $19 \times 19 \times 19$ k -point mesh.

It is known that the elastic constants are defined by means of a Taylor expansion of the total energy, $E(V, \delta)$, for the system with respect to a small strain δ on the equilibrium cell according to the following law [15]:

$$E(V, \delta) = E(V_0, 0) + V_0 \left[\sum_i \tau_i \xi_i \delta_i + \frac{1}{2} \sum_{ij} C_{ij} \delta_i \xi_j \delta_j \right], \quad (1)$$

where $E(V_0, 0)$ and V_0 are the total energy and volume of the equilibrium cell without strains, respectively, τ_i is an element in the stress tensor, and ξ_i is a factor presenting to take care of the Voigt index [16].

To calculate the elastic constants of rock-salt structure ThN, we applied three independent strains. The parametrizations that we used for these strains are given in Table I. We calculated the total energy of each strain for a number of small values of δ . These energies were then fitted to a polynomial in δ and the curvatures of the energy versus δ curve were obtained for using in Eq. (1). The elastic constants are closely related to many physical properties of solids, such as the Debye temperature, specific heat, melting temperature, and Grüneisen parameter, etc. At low temperatures, the vibrational excitations arise solely from acoustic vibrations. Hence, the Debye temperature calculated from elastic constants is the same as that determined from specific heat measurements at low temperature. The relation

between the Debye temperature (θ_D) and the average elastic wave velocity (v_m) is

$$\theta_D = \frac{h}{k_B} \left(\frac{3n}{4\pi\Omega} \right)^{1/3} v_m, \quad (2)$$

where h and k_B are Planck and Boltzmann constants, respectively, n is the number of atoms in the molecule and Ω is molecular volume. The average elastic wave velocity in the polycrystalline materials is approximately given by

$$v_m = \left[\frac{1}{3} \left(\frac{2}{v_t^3} + \frac{1}{v_l^3} \right) \right]^{-1/3}, \quad (3)$$

where $v_t = \sqrt{G/\rho}$ (ρ is the density) and $v_l = \sqrt{(3B + 4G)/3\rho}$ are the transverse and longitudinal elastic wave velocities, respectively.

After obtaining the Debye temperature at various pressures, furthermore, we performed the melting curve calculation from Debye temperatures. The calculation was based on the Lindemann melting criterion [10]. This model is based on the harmonic approximation, predicting that melting will occur when the ratio of the root mean square (rms) atomic displacement to the mean interatomic distance reaches a certain value (generally about 1/8). It can be expressed as follows

$$T_m = CV^{2/3}\theta_D, \quad (4)$$

where T_m is the melting point, C is a constant, and V is atomic volume.

III. RESULTS AND DISCUSSIONS

A. Atomic and electronic structures

In order to examine the possibility of magnetism in ThN, the spin-polarized calculations by assuming initial ferromagnetic state were carried out. We found that the ground state for ThN is non-magnetic, without any localized atomic magnetic moments, the result of which is in agreement with observed [3] paramagnetism in ThN. In this paper, the theoretical equilibrium volume V_0 , bulk modulus B and the pressure derivative B' are obtained by fitting the third-order Birch-Murnaghan equation of state (BMEOS) [17]. Our calculated lattice parameter for the cubic unit cell of ThN is $a_0 = 5.179 \text{ \AA}$, which is in good accordance with the experimental data of 5.16 \AA [18]. The bulk modulus B and its pressure derivative B'

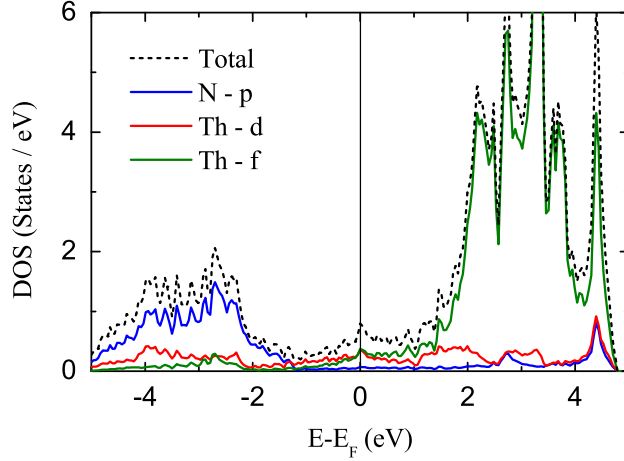


FIG. 1: (Color online) Total and site-projected orbital-resolved electronic densities of states for ThN at equilibrium. The Fermi energy is set at zero

obtained by fitting the BMEOS are 176.1 GPa and 3.9, respectively, which are also consistent with the corresponding experimental values of 175 GPa and 4.0 [19]. The calculated B for ThN is much larger than that of metallic α -Th (about 60-62 GPa [20]), i.e., a pronounced increase of structural rigidity from metal to nitride due to the direct Th-N bonding formation, which occurs as well as for other NaCl-type metal mononitrides.

The total DOS and site-projected orbit-resolved DOS (PDOS) of ThN are displayed in Fig. 1. Evidently, the conduction band is strongly marked by Th $5f$ states, with a little bit degrees of Th $6d$ and N $2p$ states. The valence band ranging from -5.5 eV to -1 eV is of mixed Th d/f and N p character. Near the Fermi level are composed by comparable contributions of Th $6d$ and $5f$ states, whereas the contributions of N $2p$ states become much smaller. Due to the observable d and f states near the Fermi energy, ThN exhibits a clear metallic behavior.

In order to further analyze the chemical bonding nature, we display in Fig. 2 the charge distribution in ThN (100) plane and list in Table II the Bader effective charges. We find the near-spherical distribution of electron density around thorium and nitrogen atoms, with rather small density value between them. This is typical for crystals with the rock-salt structure having the ionic bonding due to the charge transfer from metal to non-metal atoms. Since Bader analysis [8] is an effective tool for studying the topology of the electron density and suitable for discussing the ionic/covalent character of a compound, thus we also per-

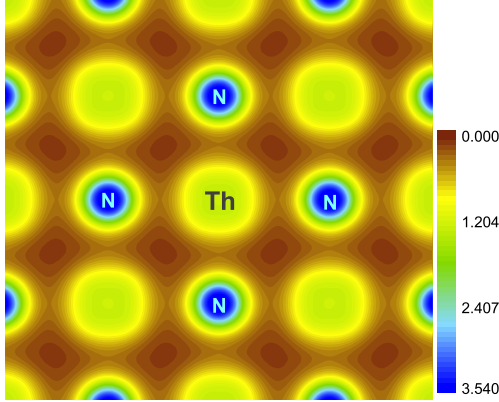


FIG. 2: (Color online) Valence charge density of ThN in (100) plane.

TABLE II: Calculated effective atomic charge and volumes according to Bader partitioning of AnN (An=Th, U, Pu).

Compound	$Q_B(A)$	$Q_B(N)$	$V_B(A)$	$V_B(N)$
	(e)	(e)	(\AA^3)	(\AA^3)
ThN	+1.82	-1.82	20.924	13.848
UN	+1.71	-1.71	18.301	11.581
PuN	+1.59	-1.59	17.713	11.757

formed the Bader effective charge calculation for ThN. For this we adopted $300 \times 300 \times 300$ charge density grids, then the spacing between adjacent grid points is 0.0172 \AA . The calculated effective atomic valence charges and volumes are listed in Table II together with the UN and PuN results for comparison. Our results show that about 1.82 electrons transfer from each Th atom to its neighboring N atoms. The effective valency in ThN then can be represented as $\text{Th}^{+1.82} \text{N}^{-1.82}$, while UN is $\text{U}^{+1.71} \text{N}^{-1.71}$ [21] and PuN is $\text{Pu}^{+1.59} \text{N}^{-1.59}$, indicating that the ionicity in ThN is somewhat stronger than that in UN and PuN, as shown in Table II.

B. Mechanical properties

For the cubic structure, there are three independent elastic constants C_{11} , C_{12} , and C_{44} . Under pressure P , the relation between the elastic constants C_{ij} and the bulk modulus B

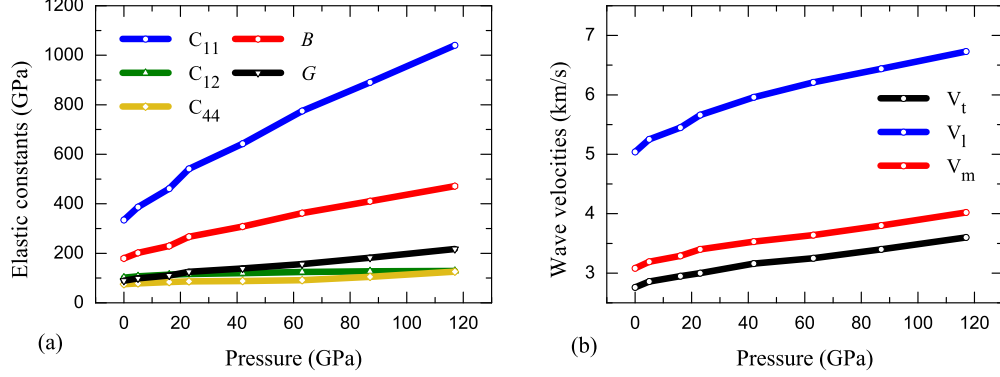


FIG. 3: (Color online) (a) Evolution with pressure of the ThN elastic constants, bulk modulus and shear modulus; (b) Evolution with pressure of the transverse elastic wave velocity v_t , longitudinal wave velocity v_l , and the average wave velocity v_m .

can be expressed as follows [22]:

$$C_{11} + 2C_{12} = 3B - P. \quad (5)$$

At zero pressure, the well-known expressions of Voigt and Reuss [16, 23, 24] bulk moduli can be re-derived. Under the Voigt approximation, the effective shear modulus G_V for cubic phase can be expressed as $G_V = \frac{C_{11} - C_{12} + 3C_{44}}{5}$, while with Reuss approximation the shear modulus can be expressed as, $G_R = \frac{5(C_{11} - C_{12})C_{44}}{4C_{44} + 3(C_{11} - C_{12})}$. Hill [25] proved that the Voigt and Reuss equations represent upper and lower limits of the true polycrystalline constants, and recommended that the shear modulus G is an arithmetic average of Voigt and Reuss approximations, i.e., $G = \frac{1}{2}(G_R + G_V)$. From that, the Young's modulus E and Poisson's ratio ν can be given by $E = \frac{9BG}{3B+G}$ and $\nu = \frac{3B-2G}{2(3B+G)}$. Using the above functions, the calculated bulk modulus B , the pressure derivative of bulk modulus B' , shear modulus G , Young's modulus E , and Poisson's ratio ν of ThN are given in Table III. For comparison, the experimental data from Ref. [19] and the theoretical FLAPW-GGA results in Ref. [26] are also presented. As can be seen from Table III, our calculated C_{12} and C_{44} are in agreement with the FLAPW-GGA results, while $C_{11} = 334.8$ GPa is smaller than the corresponding data 396.6 GPa. At ground state, the bulk modulus B derived from elastic constants is 179.4 GPa, which is well consistent with that obtained by BMEOS fitting. This value is very close to the experimental data of 175 GPa [19] but smaller than the FLAPW-GGA result of 199.9 GPa. The pressure derivative of the bulk modulus B' is 3.9, which is also in good accordance

TABLE III: Calculated elastic constants, elastic moduli, pressure derivative of the bulk modulus B' , Poisson's ratio ν , and anisotropic factor A for ThN at 0 GPa. Except B' , ν and A , all other values are in units of GPa.

Method	C_{11}	C_{12}	C_{44}	B	B'	G_V	E	ν	A
GGA	334.8	101.7	75.0	179.4	3.9	89.5	230.3	0.286	0.64
FLAPW-GGA ^a	396.6	101.5	79.9	199.9		102.4	262.5	0.281	0.54
Expt. ^b				175	4.0				

^a[26], ^b[19]

with the experimental data of 4.0. The calculated Poisson's ratio $\nu=0.286$ is consistent with the FLAPW-GGA result. With a cubic system, the elastic anisotropy factor is given by $A=\frac{2C_{44}}{C_{11}-C_{12}}$. Since that micro-cracks in materials can be easily induced by significant elastic anisotropy, so it is important to evaluate anisotropic factors in understanding their mechanical durability. Our present value of A is equal to 0.64, indicating that ThN is elastically anisotropic. As for isotropic crystals the factor A is equal to 1.0, while with any value larger or smaller than 1.10 indicating elastic anisotropy.

Besides, Figure 3(a) shows the pressure dependence of the elastic constants, bulk modulus B , and shear modulus G . One can clearly see that the elastic constants all linearly increase with pressure. The value of C_{11} , C_{12} and C_{44} are enhanced by 705 GPa, 27 GPa and 51 GPa, respectively, from 0 GPa to 117 GPa. These elastic constants satisfy the generalized elastic stability criteria for cubic crystals under pressure, i.e., $\tilde{C}_{11} > |\tilde{C}_{12}|$, $\tilde{C}_{11} + 2|\tilde{C}_{12}| > 0$, $\tilde{C}_{44} > 0$, where $\tilde{C}_{ii}=C_{ii}-P$ ($i=1, 4$) and $\tilde{C}_{12} = C_{12}+P$. The dependence of bulk modulus B and shear modulus G on pressure also linearly increase with pressure. These pressure dependence of elastic constants will be used in calculating the Debye temperature, and further predicting the melting temperatures at elevated pressures.

C. Melting curve of ThN

The melting curves of materials have great scientific and technological interest. To understand the transition between solid and liquid phases of ThN at high pressures, we will use the Lindemann criterion [Eq. (4)] to calculate the melting curve. The Lindemann criterion will be used here as a single-parameter model and the free constant C can be calculated

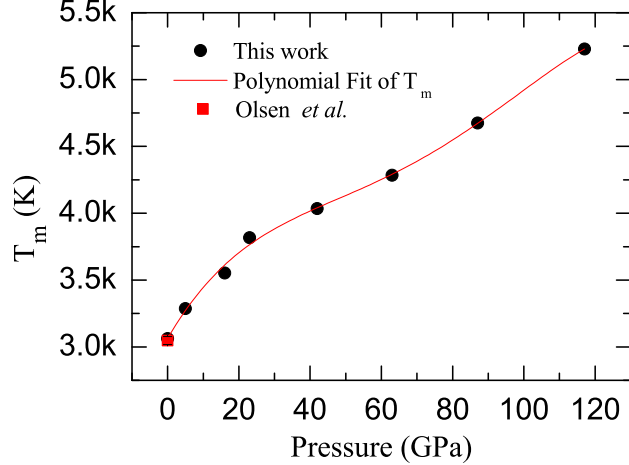


FIG. 4: (Color online) The melting temperature of ThN as a function of pressure.

from a single point. In order to perform the evolution of T_m , we should know the melting temperature T_m at $P=0$ GPa and the evolution of θ_D . On the one hand, we have known that ThN melts congruently at $2790\pm 30^\circ$ under a nitrogen pressure somewhat less than 1 atm [9]. On the other hand, using the above calculated elastic constants, we can derive the value of transverse and longitudinal elastic wave velocities, i.e., v_t and v_l , and then we can get the average wave velocity v_m by Eq. (3). From the relation between θ_D and v_m [Eq. (2)], we can finally get the value of θ_D . Figure 3 (b) shows the pressure dependence of the elastic wave velocities. One can see that all the three wave velocities increase with augmenting pressure. Through the study of evolution of Debye temperature, we can calculate the melting temperatures using the Lindeman criterion. As is shown in Fig. 4, the melting points of ThN have been calculated from ambient pressure to 117 GPa. It can be seen that the melting temperature of ThN is increased by about 2100 K from ambient pressure to 117 GPa.

D. Formation energy

The formation energy of a specific compound is defined as the difference between the total energy of the compound and of its constitutive elements. The composition reaction of ThN is as follows,



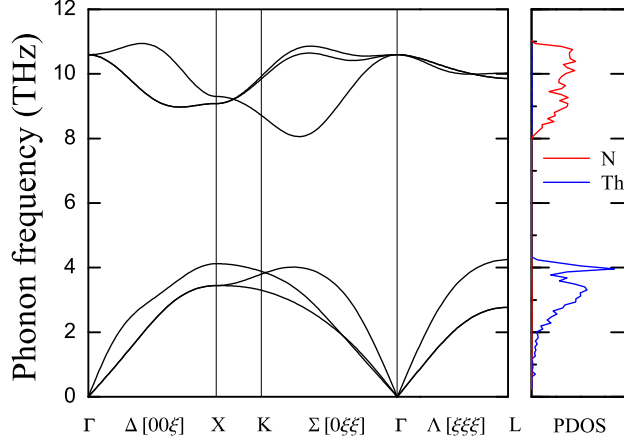


FIG. 5: (Color online) Calculated phonon dispersion curves (left panel) and corresponding projected phonon DOS (right panel) for ThN.

which yields the following expression for the formation energy:

$$E_f(\text{ThN}) = E(\text{ThN}) - (E_{\text{Th}} + \frac{1}{2}E_{\text{N}_2}). \quad (7)$$

In order to calculate the formation energy E_f , the total energy of ThN, α -Th and N_2 dimer should be calculated. Density-functional theory is known to overestimate the binding energy E_b of N_2 dimer, so it will result in an underestimation of the present reaction energy via the E_{N_2} term. However, this error can be remedied by shifting the energy of N_2 so as to give the experimental binding energy. The experimental E_b of N_2 is 9.9 eV [27]. In the GGA the E_b is overestimated by about 0.7 eV/ N_2 . The formation energy E_f is -2.14 eV/atom with the correction in the E_{N_2} term. This value is somewhat higher than the experimentally measured enthalpy of formation $\Delta_f H = -1.81$ eV/atom at room temperature [28]. Since the formation energy calculated here does not take into account the temperature, therefore, it can only give insight into the stability of the compounds at low temperatures.

E. Phonon dispersion curve

In calculating the phonon dispersion curves and the phonon density of states, the Hellmann-Feynman theorem and the direct method [29] are employed. For the BZ integration, the $3 \times 3 \times 3$ Monkhorst-Pack k -point mesh is used for the $2 \times 2 \times 2$ ThN supercell which contains 64 atoms. In order to calculate the Hellmann-Feynman forces, we displace two

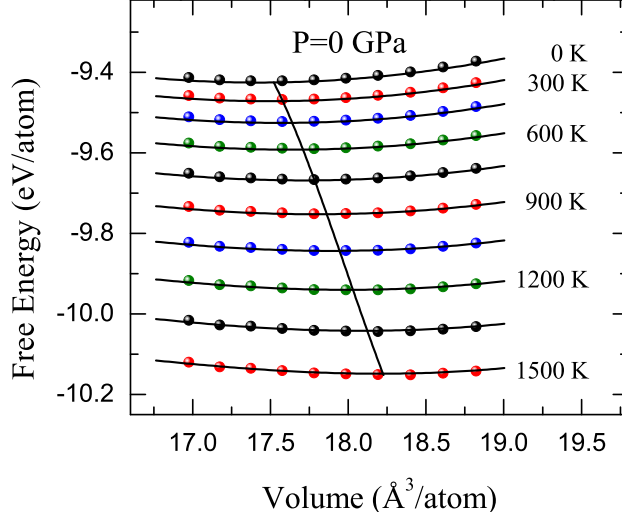


FIG. 6: (Color online) Dependence of the Helmholtz free energy $F(T, V)$ on crystal volume at various temperatures and the locus of the minimum of the free energy for ThN.

atoms (one Th and one N atoms) from their equilibrium positions and the amplitude of all the displacements is 0.03 \AA . The calculated phonon dispersion curves along $\Gamma - X - K - \Gamma - L$ directions is displayed in Fig. 5. For rock-salt type ThN, there are only two atoms in its formula unit, therefore, six phonon modes exist in the dispersion relations. The projected phonon DOS for ThN is also plotted in Fig. 5. Because of the fact that the thorium atom is heavier than the nitrogen atom, the phonon DOS splits into two parts with an evident gap: one part is in the range of 0-4 THz where the vibrations of thorium atoms are dominant; the other part is in the domain of 8-11 THz where the vibrations mainly come from nitrogen atoms. Our calculated optical frequency at Γ is about 10.6 THz, and this value is very close to the experimental value of 10.3 THz [18]. The phonon dispersion illustrates the stability of ThN, and further indicates that our following thermodynamic calculations are reliable.

F. Thermodynamic properties

The Helmholtz free energy F in QHA is investigated as follows:

$$F(V, T) = E(V) + F_{ph}(V, T) + F_{ele}(V, T), \quad (8)$$

where $E(V)$ stands for the ground-state cold energy, $F_{ph}(V, T)$ is the phonon free energy at a given unit cell volume V , and F_{ele} is electron excitation energy. Under QHA, the $F_{ph}(V, T)$

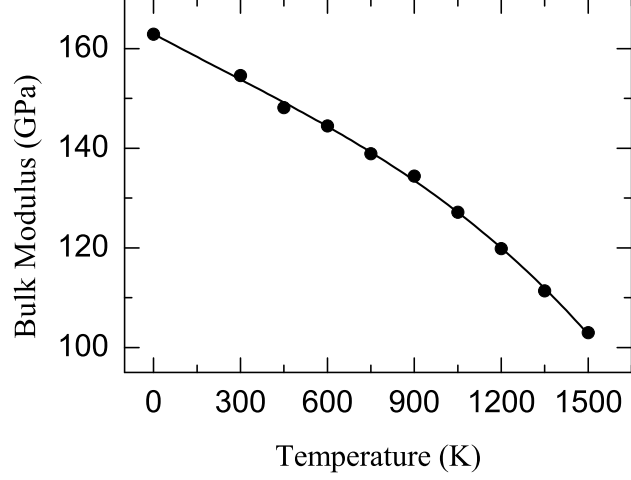


FIG. 7: (Color online) Temperature dependence of the bulk modulus for ThN.

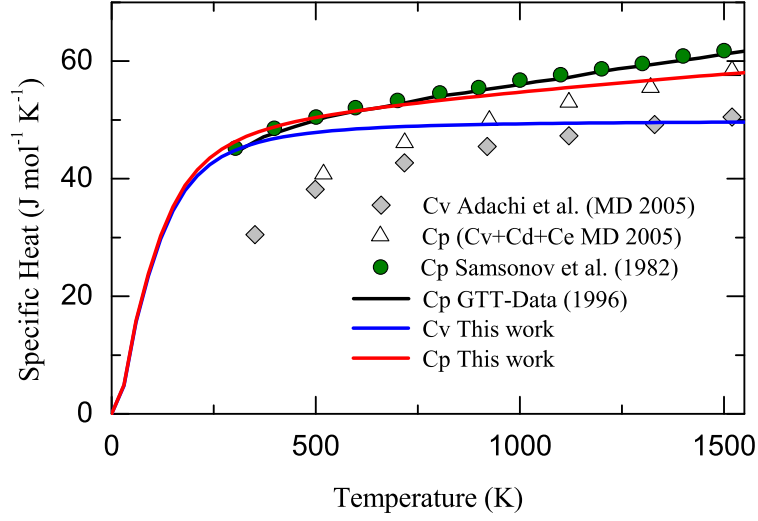


FIG. 8: (Color online) Specific heat capacities of ThN. Experimental data from Refs. [30, 31] and theoretical results from Ref. [32] are also displayed for comparison.

can be calculated from phonon DOS $g(\omega)$ by

$$F_{ph}(V, T) = k_B T \int_0^\infty g(\omega) \ln \left[2 \sinh \left(\frac{\hbar \omega}{2k_B T} \right) \right] d\omega, \quad (9)$$

where $\omega = \omega(V)$ depends on volume and thus Equation (9) contains some effect of anharmonics. F_{ele} in Eq. (8) can be obtained from the energy and entropy contributions, i.e., $E_{ele} - TS_{ele}$. The electronic entropy S_{ele} is of the form

$$S_{ele}(V, T) = -k_B \int n(\varepsilon, V) [f \ln f + (1 - f) \ln (1 - f)] d\varepsilon, \quad (10)$$

where $n(\varepsilon)$ is electronic DOS, and f is the Fermi-Dirac distribution. While the energy E_{ele} due to the electron excitations takes the following form

$$E_{ele}(V, T) = \int n(\varepsilon, V) f \varepsilon d\varepsilon - \int^{\varepsilon_F} n(\varepsilon, V) \varepsilon d\varepsilon, \quad (11)$$

where ε_F is the Fermi energy.

The calculated free energy $F(V, T)$ curves of ThN for temperature ranging from 0 up to 1500 K are shown in Fig. 6. The locus of the equilibrium lattice parameters at different temperature T are also presented. The equilibrium volume $V(T)$ and the bulk modulus $B(T)$ are obtained by BMEOS fitting. Figure 7 shows the temperature dependence of the bulk modulus B . Clearly, the bulk modulus $B(T)$ decreases along with the increase of temperature. This kind of temperature effect is very common for compounds and metals. Besides, the specific heat at constant volume C_V can be directly calculated through

$$C_V = \left(\frac{\partial F}{\partial T}\right)_V = k_B \int_0^\infty g(\omega) \left(\frac{\hbar\omega}{k_B T}\right)^2 \frac{\exp \frac{\hbar\omega}{k_B T}}{(\exp \frac{\hbar\omega}{k_B T} - 1)^2} d\omega, \quad (12)$$

while the specific heat at constant pressure C_P can be evaluated by the thermodynamic relationship $C_P - C_V = \alpha_V^2(T) B(T) V(T) T$, where the isobaric thermal expansion coefficient can be calculated according to the formula $\alpha_V(T) = \frac{1}{V} \left(\frac{\partial V}{\partial T}\right)_P$. Calculated C_V and C_P of ThN are displayed in Fig. 8. For comparison, the experimental data from Refs. [30, 31] and the theoretical molecular dynamics (MD) results by Adachi *et al.* [32] are also presented. In general, our calculated values of C_V and C_P are both higher than the corresponding MD results up to 1500 K. However, our calculated C_P , including both lattice and conduction electron contributions, agrees well with experimental results in a wide temperature domain with a tiny discrepancy of 4 J/mol·K at 1500 K.

IV. CONCLUSION

In summary, we have performed systematic first-principles calculations on the structural, electronic, mechanical, and thermodynamic properties of ThN. Within the GGA method, the ground state structure of ThN can be well produced. Our calculated lattice constant is in good accordance with the experimental data, within 0.05% error. Calculated electronic density of states show the important contributions of Th $6d$ and $5f$ states to the Fermi-level occupation. The Bader effective charges of ThN can be expressed as $\text{Th}^{+1.82}\text{N}^{-1.82}$, which

is indicated to be more ionic when compared to UN and PuN. The mechanical analysis has been carried out, showing that the rock-salt type ThN is mechanically stable in a wide range of pressures. Also, we have presented the melting curve of ThN from ambient pressure to 117 GPa by utilizing the Lindemann criterion. The calculated phonon dispersion of ThN is stable, confirming the dynamic stability. Under the QHA method, our calculated specific heat, including both lattice and conduction electron contributions, agrees well with experimental results. We expect that these calculated results will be useful for the application of thorium nitrides in the Generation-IV reactor and nuclear industry.

Acknowledgments

This work was supported by NSFC under Grants No. 51071032 and the Foundations for Development of Science and Technology of China Academy of Engineering Physics under Grant No. 2009B0301037.

-
- [1] Proc. Global Future Reactor Technologies (Tsukuba, Japan, Oct. 2005)
 - [2] H.J. Matzke, Diffusion Processes in Nuclear Materials, (Amsterdam: Elsevier, 1992)
 - [3] H. Kleykamp, Thorium Carbides. Gmelin Handbook of Inorganic and Organometallic Chemistry, eighth ed. Thorium supplement, vol. C6, Springer, Berlin, 1992.
 - [4] A.H.M. Evensen, R. Catherall, P. Drumm, P. Van Duppen, O.C. Jonsson, E. Kugler, J. Lettry, O. Tengblad, V. Tikhonov, H.L. Ravn, Nuclear Inst. Method. Phys. Res. B **126** 160 (1997).
 - [5] A.A. Bauer, Reactor Technol. **15**, 87 (1972).
 - [6] M.S.S. Brooks, J. Phys. F: Met. Phys. **14**, 857-871 (1984).
 - [7] I.R. Shein, K.I. Shein, N.I. Medvedeva, and A.L. Ivanovskii, Physica B **389**, 296 (2007).
 - [8] R. Bader, Atoms in Molecules: A Quantum Theory, Oxford University Press, New York, (1990).
 - [9] W. M. Olson and R. N. R. Mulford, J. Phys. Chem, **69**, 4, April 1965.
 - [10] F.R. Lindemann, Z. Phys. **11**, 609 (1910).
 - [11] G. Kresse, J. Furthmüller, Phys. Rev. B **54**, 11169 (1996).
 - [12] P. E. Blöchl, Phys. Rev. B **50**, 17953 (1994).

- [13] J.P. Perdew, K. Burke, Y. Wang, Phys. Rev. B **54**, 16533 (1996).
- [14] H.J. Monkhorst, J.D. Pack, Phys. Rev. B **13**, 5188 (1976).
- [15] L. Fast, J.M. Wills, B. Johansson, O. Eriksson, Phys. Rev. B **51**, 17431 (1995).
- [16] W. Voigt, Lehrbuch der Kristallphysik, Teubner, Leipzig, (1928).
- [17] F. Brich, Phys. Rev. **71**, 809 (1947).
- [18] F. A. Wedgwood, J. Phys. C: Solid State Phys. **7**, 3203 (1974).
- [19] L. Gerward, J. S. Olsen, U. Benedict, J. P. Itié, J.C. Spirlet, J. Appl. Cryst. **18**, 339 (1985).
- [20] K. Hachiy, Y. Ito, Physica B, **262**, 233 (1999).
- [21] Y. Lu, B. T. Wang, R. W. Li, H. Shi, and P. Zhang, J. Nucl. Mater. (in press).
- [22] G.V. Sin'ko, N.A. Smirnow, J. Phys.: Condens. Matter **14**, 6989 (2002).
- [23] A. Reuss, Z. Angew. Math. Mech. **9**, 49 (1929).
- [24] D. L. Preston and D. C. Wallace, Solid State Commun. **81**, 277 (1992).
- [25] R. Hill. Phys. Soc. London **65**, 350 (1952).
- [26] I.R. Shein, A.L. Ivanovskii, J. Struct. Chem **49**, 2, 348-370 (2008).
- [27] C. Stampfl and C. G. Van de Walle, Phys. Rev. B **59**, 5521 (1999).
- [28] D. Sedmidubský, R.J.M. Koningsb, P. Novák, J. Nucl. Mater. **344** 40-44 (2005).
- [29] K. Parlinski, Z.Q. Li, Y. Kawazone, Phys. Rev. Lett, **78**, 4063 (1997).
- [30] G.V. Samsonov, I.M. Vinitkii, Handbook of Refractory Compounds, 1982.
- [31] The SGTE Pure Substance and Solution Databases, GTT-Data Services, 1996.
- [32] J. Adachi, K. Kurosaki, Masayoshi Uno, Shinsuke Yamanaka, J. Alloy. Compd. **394**, 312-316 (2005).